

## RESEARCH ARTICLE

# A comparison of an operational wave–ice model product and drifting wave buoy observation in the central Arctic Ocean: investigating the effect of sea-ice forcing in thin ice cover

Takehiko Nose<sup>1</sup>, Jean Rabault<sup>2</sup>, Takuji Waseda<sup>1</sup>, Tsubasa Kodaira<sup>1</sup>, Yasushi Fujiwara<sup>1,3</sup>, Tomotaka Katsuno<sup>1</sup>, Naoya Kanna<sup>4</sup>, Kazutaka Tateyama<sup>5</sup>, Joey Voermans<sup>6</sup> & Tatiana Alekseeva<sup>7,8</sup>

<sup>1</sup>Department of Ocean Technology, Policy and Environment, Graduate School of Frontier Sciences, the University of Tokyo, Kashiwa, Chiba, Japan

<sup>2</sup>Norwegian Meteorological Institute, IT Department, Oslo, Norway

<sup>3</sup>Graduate School of Maritime Sciences, Kobe University, Kobe, Japan

<sup>4</sup>Atmosphere and Ocean Research Institute, the University of Tokyo, Kashiwa, Chiba, Japan

<sup>5</sup>Kitami Institute of Technology, Kitami, Hokkaido, Japan

<sup>6</sup>University of Melbourne, Melbourne, Australia

<sup>7</sup>Arctic and Antarctic Research Institute, Saint Petersburg, Russia

<sup>8</sup>Space Research Institute, Moscow, Russia

## Abstract

A prototype OpenMetBuoy (OMB) was deployed alongside a commercial buoy in the central Arctic Ocean, north of the Laptev Sea, where there are historically no wave observations available. The inter-buoy comparison showed that the OMB measured wave heights and periods accurately, so the buoy data were used to study the predictability of a wave–ice model. The first event we studied was when both buoys observed a sudden decrease in significant wave heights  $H_{m0}$ , which was caused by the change of wind directions from along the ice edge to off-ice wind. The Arctic Ocean Wave Analysis and Forecast wave–ice model product (ARC MFC) underestimated the  $H_{m0}$  on the account of the fetch being constrained by the inaccurate model representation of an ice tongue. The second case was an on-ice wave event as new ice formed. In this instance, the ARC MFC wave–ice model product largely underestimated the downwind buoy  $H_{m0}$ . Model sea-ice conditions were examined by comparing the ARC MFC sea-ice forcing with the neXtSIM sea-ice model product, and our analysis revealed the ARC MFC did not resolve thin ice thickness distribution for ice types like young and grey ice, typically less than 30 cm. The ARC MFC model's wave dissipation rate has a sea-ice thickness dependence and overestimated wave dissipation in thin ice cover; sea-ice forcing that can resolve the thin thickness distribution is needed to improve the predictability. This study provides an observational insight into better predictions of waves in marginal ice zones when new ice forms.

To access the supplementary material, please visit the article landing page

## Keywords

OpenMetBuoy; ARC MFC wave–ice model; neXtSIM sea-ice model; wave–ice interaction; MIZ wave predictability; ice thickness

## Correspondence

Takehiko Nose, Department of Ocean Technology, Policy and Environment, Graduate School of Frontier Sciences, University of Tokyo, 5–1–5 Kashiwanoha, Kashiwa, Chiba, Japan. E-mail tak.nose@edu.k.u-tokyo.ac.jp

## Abbreviations

AMSR2: Advanced Microwave Scanning Radiometer 2  
ARC MFC: Arctic Ocean Wave Analysis and Forecast (produced by the Copernicus Marine Arctic Monitoring and Forecast Center)  
CMEMS: Copernicus Marine Environment Monitoring Service  
GNSS: global navigation satellite system  
GPS: global positioning system  
ECMWF HRES: High Resolution Forecast (produced by the European Centre for Medium-range Weather Forecasts)  
HYCOM: Hybrid Coordinate Ocean Model (sponsored by the National Ocean Partnership Program)  
IMU: inertial measurement unit  
MIZ: marginal ice zone  
NABOS: Nansen and Amundsen Basins Observational System (part of the Arctic Observing Network)  
neXtSIM: sea-ice forecast (produced by the Nansen Environmental and Remote Sensing Center)  
OMB: OpenMetBuoy  
OSI SAF: Ocean and Sea Ice Satellite Application Facility  
OSTIA: Operational Sea Surface Temperature and Ice Analysis (produced by the UK Met Office)  
SIC: sea-ice concentration  
SIT: sea-ice thickness  
TOPAZ4: Towards an Operational Prediction System for the North Atlantic European Coastal Zones (version 4) data assimilation system

## Introduction

Wave–ice interaction research is attracting renewed attention because of declining Arctic Ocean sea-ice cover and a conjecture that waves in ice have an influence on the climate system (Squire 2018, 2020). Despite recent advancement in model parameterization since one of the most intensive waves-in-ice data collection campaigns of Thomson et al. (2018), incorporating the effects of waves in sea-ice models and vice versa remains a challenging problem. In MIZs, where the sea-ice field is heterogeneous and waves are most dynamic, the problem becomes even more challenging as accurate sea-ice condition is difficult to obtain. Uncertainty arising from SIC estimates (from passive microwave radiometers) used as sea-ice forcing for wave–ice models can even overwhelm the uncertainty of wave–ice interaction parameterizations (Nose et al. 2020). In light of these challenges, it can be argued that more observations are needed to better understand wave–ice interaction physics and improve the predictability of ocean waves in MIZs.

Utilizing the recent advances of inexpensive electronics and their open-source philosophy, Rabault et al. (2022) developed and introduced a low-cost, easy to build wave–ice buoy called OMB. The OMB applies a 6 degrees of freedom IMU to measure vertical ocean surface motion. The vertical surface oscillation can then be used to obtain power spectral density, from which integrated wave statistics like the wave height and periods can be calculated. In September 2021, our research team joined the NABOS campaign (NABOS no date) on board the RV *Akademik Tryoshnikov*, and we deployed a prototype of the OMB alongside a commercial wave buoy in the central Arctic Ocean, where there are historically no wave observations available. In this study, we evaluated our prototype OMB with a commercial wave buoy; we then used the buoy data set to study the wave–ice model predictability in this region.

To simulate the ice effects on waves, we first need to consider the length scale between  $\lambda$  and  $D$  (Linton 2010), where  $D$  could be considered the diameter of ice floes and is the wavelength. For an ice sheet and grease ice where  $\lambda < D$  and  $\lambda \gg \text{SIT}$ , the sea ice can be modelled as a thin elastic ice layer where waves propagate under ice, and the ocean–ice interface is where the dissipation occurs. When  $\lambda \approx D$ , wave attenuation is understood to be dominated by a conservative process known as the scattering mechanism, which was first observed by Wadhams (1975). When  $\lambda > D$ , waves propagate through smaller sea-ice floes, and dissipation occurs in many forms (Squire 2018); this type of ice cover can be modelled as a semi-infinite viscous ice layer, in which effective material properties can be tuned to reproduce the aggregate effect of various sea-ice effects on waves (Squire 2018).

The  $\lambda > D$  regime is primarily observed in the MIZ. This is the length scale of interest to our wave buoy observation because the ice charts indicated that the wave buoys were located near and in new and young ice, with typical thickness less than 30 cm, during the observation period (see Supplementary material). For the purpose of a model–observation comparison, we used an operational model called ARC MFC, with data from the specific product ARCTIC\_ANALYSIS\_FORECAST\_WAV\_002\_014 downloaded on 18 January 2022.

Because the ARC MFC model’s wave dissipation parameterization (Sutherland et al. 2019) is suited for modelling waves in the MIZ thin ice cover, we expect reasonable model agreement with the observation. Our objective in this study is to elucidate the predictability of the ARC MFC wave–ice model in the central Arctic Ocean by applying the drifting wave buoy observations and two other model products: ECMWF HRES (wave) and neXt-SIM (sea ice). Specifically, we focus on how sea-ice edge and SIT representations in the sea-ice forcing affect wave predictions when new ice is forming.

## Drifting wave buoy observation

### Wave buoy sensor and platform description

During the 2021 NABOS campaign, we deployed the first prototype of the OMB developed by Rabault et al. (2022), to which we refer herein as the Zeni-v2021, alongside a Sofar Spotter, herein referred to as SPOT-1386. Both Zeni-v2021 and SPOT-1386 buoys measure ocean surface motion, but they use different technology.

The Zeni-v2021 was recently introduced by Rabault et al. (2022). The OMB electronic components for detecting ocean surface motion are a 6 degrees of freedom accelerometer and gyroscopic IMU manufactured by ST (model ISM330DHCX). The attitude heading reference system correction via sensor fusion of three-axis accelerations and angular rates produces true vertical acceleration (Rabault et al. 2022), which is integrated twice to estimate the surface elevation.

The OMB ‘buoy’ is a sensor unit that is housed in a waterproof enclosure (e.g., figure A1 by Rabault et al. 2022); it is not designed as a floating platform in water. The primary deployment method of OMBs is that the sensor unit is placed on an ice floe, and the ice floe becomes the sensor’s floating platform (hence, the term ‘wave–ice buoy’). At the time of the buoy preparation, in July 2021, the sea-ice extent was low, nearly as reduced as the 2012 record low sea-ice extent. (However, by August, the sea-ice extent had plateaued, resulting in limited opportunities for open-water deployment. See Arctic Data Archive System [2023] for sea-ice extent images.) An alternative

deployment method was devised by housing the sensor in a floating platform. The ad hoc platform was a Zenilite GPS tracker enclosure, whose design allowed it to house the OMB electronic components (see Appendix B, Rabault et al. 2022). The Zenilite GPS drifting buoy has a diameter of 340 mm, is 300 mm in height and weighs about 6 kg.

SPOT-1386 is a commercially sold drifting wave buoy; it is a proven technology with thousands of them currently deployed in the world oceans. The dimensions are similar to the Zenilite GPS drifter, which are 420 mm wide by 310 mm high and weigh 5.3 kg (7.4 kg with a ballast); therefore, SPOT-1386 is an appropriate benchmark for Zeni-v2021. Spotters’ proprietary firmware uses a GPS/GNSS receiver to get the device horizontal and vertical displacements.

### Buoy deployment

The wave buoys were deployed adjacent to an ice edge in the central Arctic Ocean, north of the Laptev Sea (81.915°N, 118.763°E) at about UTC 05:05 on 15 September 2021. The deployment location is shown in Fig. 1, and the sea-ice conditions as observed onboard the ship on the day of the buoy deployment are shown in Fig. 2. The SPOT-1386 battery life at high latitudes without a solar charge is approximately 10 days; as such, the co-located deployment duration only lasted between 15 and 29 September. The buoy tracks for this period are shown in Fig. 1a, which is overlaid with the AMSR2 SIC (Hori et al. 2012) contours.

The primary motive for the buoys being deployed at the same location was to validate Zeni-v2021 against SPOT-1386, and we anticipated that the buoys would measure analogous wave signal for at least several days. For example, Waseda et al. (2018) and Nose et al. (2018) describe the trajectories and wave statistics of two buoys deployed at the same location in the ice-free Beaufort Sea in 2016; the buoys drifted along similar tracks for about 13 days, during which time, they measured analogous wave statistics. However, we observed that the Zeni-v2021 and SPOT-1386 wave heights began deviating slightly merely 12 hours after the buoys were deployed. Two days after deployment, wave heights and periods varied considerably between the two buoys, which indicates that the measured waves’ evolution did not occur entirely over open ocean, that is, sea ice affected how the waves evolved.

### Co-located wave buoy measurements in thin ice field

**Overview of the wave data.** Figure 3 presents an overview of the co-located buoy observation: the buoy distances, and wind, wave and SIC conditions. Here, wave statistics derived from the vertical surface elevation are significant wave height  $H_{m0} = 4\sqrt{m_0}$ , where  $m_0 = \int_{f_0}^{f_1} S(f)df$  and wave periods (peak period  $T_p$ , which is the inverse frequency of peak  $S(f)$  and  $-1$  moment period, also known as energy mean wave period,  $T_{0m1} = \frac{\int_{f_0}^{f_1} f^{-1} S(f)df}{m_0}$ ).

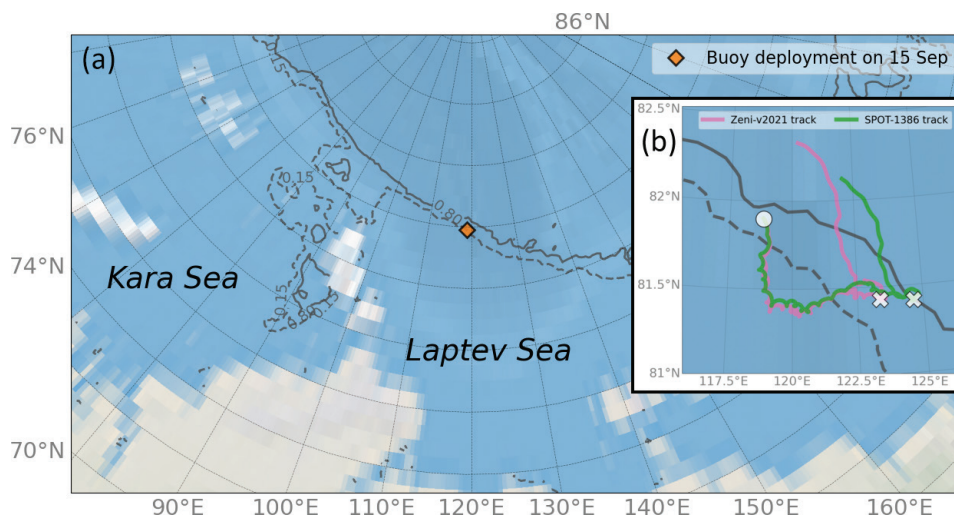


**Fig. 1** (a) The co-located wave buoys were deployed in the Arctic Ocean on 15 September 2021. (b) The Zeni-v2021 and SPOT-1386 trajectories between 15 September (white dot) and 29 September are shown. The white crosses show approximate location when the visible inertial oscillation stopped on 25 September 2021, which could indicate a change in ocean surface conditions. The dashed and solid lines in (a) 15 September and (b) 25 September indicate the 0.15 and 0.80 AMSR2 SIC contours, respectively.

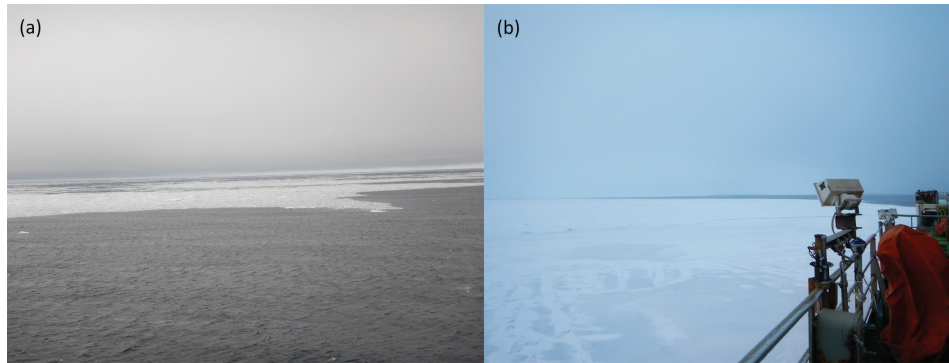


**Fig. 2** Sea-ice conditions encountered during the cruise on 15 September 2021 after the buoys were deployed: (a) grey ice and (b) grey-white ice, both belonging to the young ice category.

The notations are frequency spectrum  $S$  and frequency  $f$ . The integration range was  $(f_0, f_1)$  for  $n$ th spectral moments  $m_n$ , where  $f_1 = 0.308$  Hz. Zeni-v2021 data were affected by the noise floor that was elevated whilst the buoy was drifting in open water until about 25 September; the elevated noise floor is analogous to the observation by Waseda et al. (2017), Waseda et al. (2018) and Nose et al. (2018) and seems to accompany IMU-based wave sensors housed in a relatively small floating platform. The same ideal filter method as used by Waseda et al. (2017), Waseda et al. (2018) and Nose et al. (2018) was implemented to derive the wave statistics. As such,  $f_0$  was not a constant and depended on the ideal-filter cut-off frequency. The Zeni-v2021 integration range  $(f_0, f_1)$  was matched in the SPOT-1386 wave statistics calculation. It is noteworthy that the elevated noise floor was observed until 25 September, which roughly coincides with the time when the inertial oscillation visible in Fig. 1a seemingly stopped (Figs. 1, 3).

**Inter-buoy comparison.** It is apparent in the  $H_{m_0}$  panel of Fig. 3 that, despite the buoys having similar drifting trajectories for the first half of the deployment,  $H_{m_0}$  began to vary slightly between them after half a day and considerably after just two days. As we will show throughout the paper, the variability likely indicates that the wave evolution was modified by the sea-ice fields via one of the following effects: (1) waves are attenuated as they propagate into the ice-cover medium; (2) lateral boundary conditions are imposed by the ice fields and affect the wave evolution over the effective fetch.

Although we discuss (below) the possibility that the effective fetch at the buoys' location after 12 hours of deployment was already affected by the sea-ice lateral boundary, we aim to consolidate the general inter-buoy agreement when the buoys were in close proximity. Scatter for  $H_{m_0}$  and  $T_{0m1}$  is plotted in Fig. 4. The markers were grouped by an arbitrary buoy distance threshold of 5 km to demonstrate that the buoys' wave statistics agreed better when the distance between them was shorter, that is, the

effect of the sea-ice field on wave evolution is less for shorter distances. Indeed, the blue markers, indicating the data when the between-buoy distance was  $<5$  km, in both panels are clustered closer to the black dotted agreement line than the red markers. Furthermore, as was shown in the left panel of Fig. 7 by Rabault et al. (2022), the spectra agreed well immediately after the buoys were deployed.

Whilst precise Zeni-v2021 validation with SPOT-1386 was impeded by the growing sea-ice fields, we showed that the Zeni-v2021 measurement quality seems sufficiently adequate when the wave evolution was less altered by the sea-ice field (when the distances between them were short). As such, we used the wave events observed by the co-located buoy measurements to evaluate the operational ARC MFC wave–ice model predictability.

## Numerical models

### ARC MFC wave–ice model

**The wave–ice interaction parameterization.** The ARC MFC wave–ice model is an operational wave model product for the Arctic Ocean and includes a wave–ice interaction parameterization, that is, the model can simulate wave propagation in sea-ice cover. Medium-range forecast and analysis are distributed via the CMEMS platform.

The ARC MFC wave–ice interaction is based on the work of Sutherland et al. (2019). They modelled wave dissipation with a two-layer sea-ice model: the top layer is modelled like a thin film that has no horizontal motion with thickness  $(1-\varepsilon)h_i$ , whilst the bottom layer is modelled as a moving viscous layer. Here,  $h_i$  is the ice thickness. Sutherland et al. (2019) describe that the  $\varepsilon$  coefficient is related to ice permeability at the microscopic scale and is a function of ice temperature, salinity and ice volume fraction. The assumption of a highly viscous top layer is similar to Weber (1987), who derived a well-known wave dissipation solution by modelling the thin

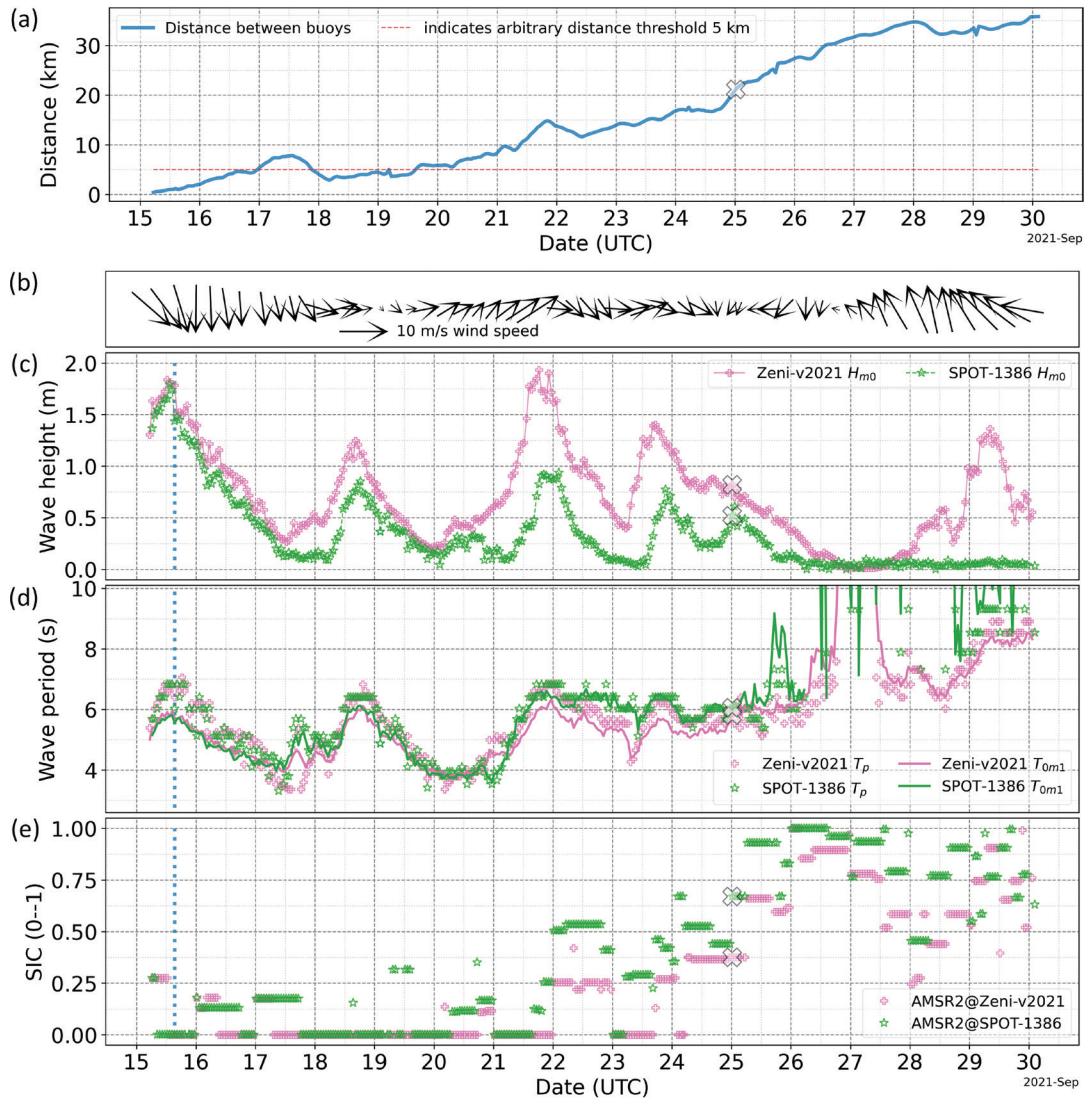


**Fig. 3** An overview of the co-located wave buoy measurements: (a) a time series of buoy distances; (b) the ECMWF HRES atmospheric forecast wind vector extracted at the Zeni-v2021 location; (c) the buoy significant wave height  $H_{m0}$ ; (d) energy mean and peak wave periods  $T_{0m1}$  and  $T_p$ ; (e) the AMSR2 SIC extracted at the buoy locations. The blue dotted lines indicate when the buoys'  $H_{m0}$  began to deviate slightly. The white crosses correspond to the approximate times when the inertial oscillations seemingly stopped (Fig. 1).

ice cover as an inextensible layer that halts the horizontal motion of the fluid layer underneath. The model by Sutherland et al. (2019) could be considered an extension of the Weber (1987) model. In the latter, the dissipation rate is  $\alpha \propto K_{35} f^{3.5}$  where  $K_{35}$  is a constant. The model by Sutherland et al. (2019) also has a frequency dependence, but they also included an ice thickness dependence to the dissipation rate:  $\alpha \propto K_{40} f^4$ , where  $K_{40}$  is a function of ice thickness. A more thorough discussion on the various dissipation rates in the literature is provided by Waseda et al. (2022).

Sutherland et al. (2019) developed their model on the basis of a scaling argument as they derived that the

viscosity scales with SIT,  $\nu \propto h_i$ , which led to spatial wave dissipation as a function of ice thickness and frequency:  $\alpha \propto h_i f^4$ . The dissipation rate is parameterized in equation 16 by Sutherland et al. (2019) as:

$$\alpha = \frac{1}{2} \Delta_0 \varepsilon h_i k^2, \tag{1}$$

where  $\Delta_0 \approx 1$ . In the CMEMS Quality Information Document (Bohlinger et al. 2022), the dissipation rate is denoted as,  $\alpha = C_d h_i k^2$ , where they state that  $C_d$  is a tuning parameter and is determined by the best fit to the observation obtained from the ice-covered fjord, Tempelfjorden, in Svalbard, in 2018. Note that when  $\varepsilon = 0$  (or  $C_d$ ), the model may behave

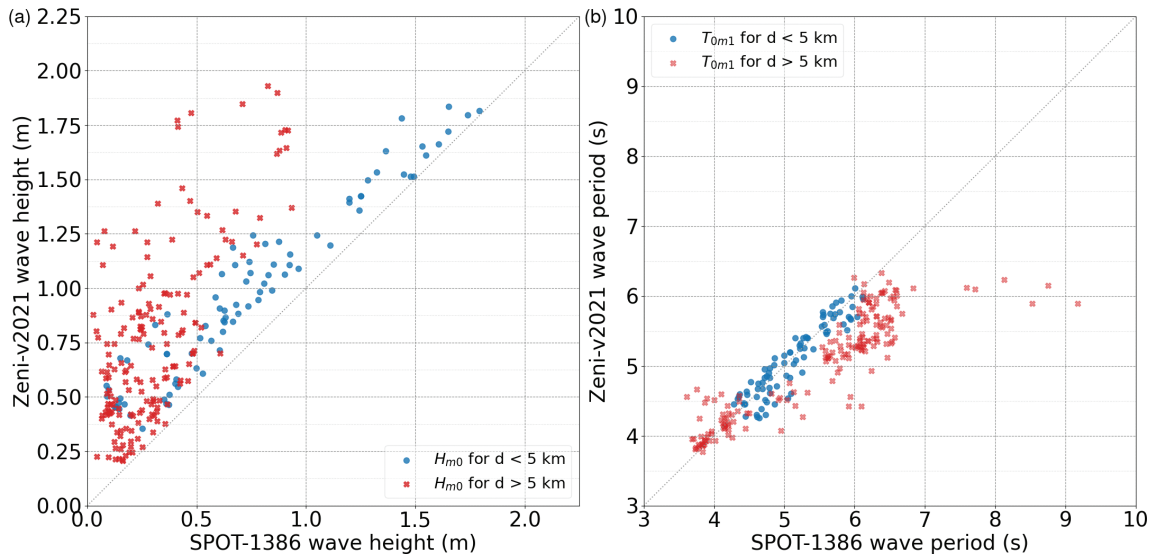


**Fig. 4** Scatterplots of Zeni-v2021 and SPOT-1386 from 15 to 25 September: (a) the  $H_{m0}$  (m) and (b) the  $T_{0m1}$  (s). The date of 25 September was chosen to avoid comparing wave periods that were affected by the buoy noise floor (see the wave periods shown in Fig. 3). The marker colours were grouped using an arbitrary buoy distance threshold: blue represents a distance less than 5 km and red greater than 5 km apart. The blue markers tend to cluster near the agreement lines (black dotted lines).

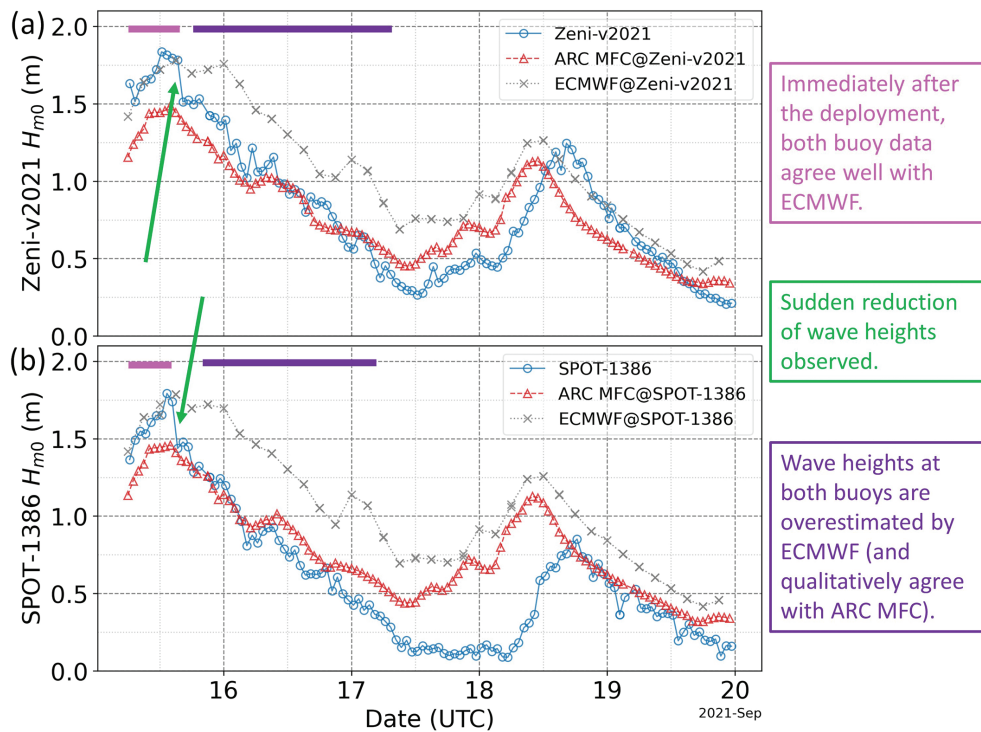


**Fig. 5** Significant wave height  $H_{m0}$  time series comparing the models (grey and red symbols) with the (a) Zeni-v2021 and (b) SPOT-1386 buoy observation (blue symbols) between 15 and 19 September 2021 when the buoy distances were generally less than 5 km after the deployment. The missing values in the ECMWF HRES wave forecast are due to ice masks (grid cells with SIC > 0.30). The pink bars indicate when the buoy observation agreed with the ECMWF HRES wave forecast. The green arrows show when a sudden reduction in the wave heights was observed. The purple bars indicate when the buoy observation agreed qualitatively with the ARC MFC wave-ice model.

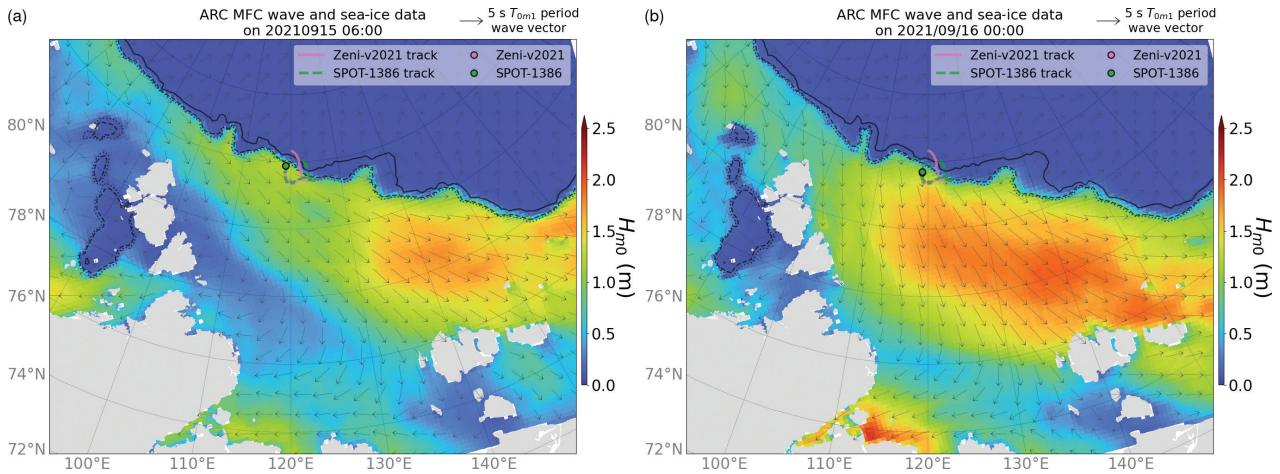


**Fig. 6** ARC MFC wave fields showing how the fetch orientation of the Zeni-v2021 and SPOT-1386 trajectories changed from (a) along the ice edge immediately after the deployment at 06:00 on 15 September 2021 to (b) off-ice by 00:00 on 16 September. Colours indicate the  $H_{m0}$ , whilst the grey vectors correspond to mean wave directions with the vector lengths scaled by  $T_{0m1}$ . The SIC contour lines are 0.15 (dotted), 0.30 (dashed) and 0.80 (solid).

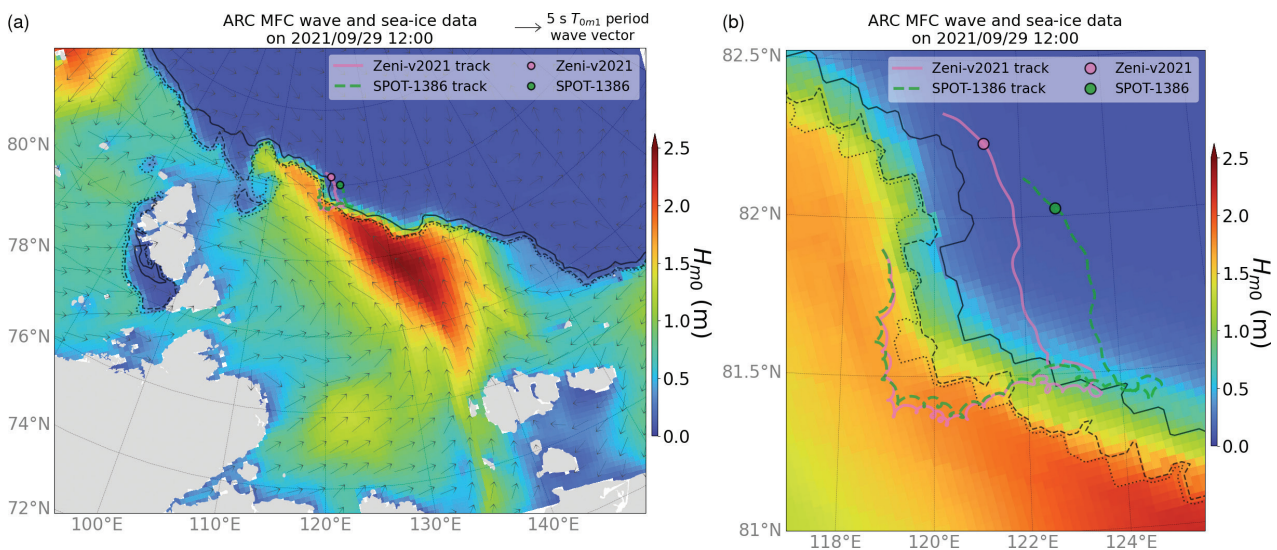


**Fig. 7** ARC MFC ice and wave fields during the wave event on 29 September 2021 when Zeni-v2021 measured ca. 1.3 m  $H_{m0}$ , but the model showed no waves. (a) The wave conditions in which the colours indicate  $H_{m0}$ , whilst the grey vectors correspond to mean wave directions with the vector lengths scaled by  $T_{0m1}$ . (b) A zoomed-in view of (a) near the buoys. The SIC contour lines are 0.15 (dotted), 0.30 (dashed) and 0.80 (solid).

like the Weber (1987) model if the boundary layer in the fluid is implemented (not done so in the model by Sutherland et al. [2019], yet). Lastly, the dissipation rate  $\alpha$  is used to estimate the dissipated wave spectrum as follows:

$$S(f) = S_0(f)e^{-\alpha x}, \tag{2}$$

where  $S_0$  is the incoming wave spectrum and  $x$  is a distance between the two points.

The wave part of the ARC MFC wave–ice model is based on Met Norway’s version of WAM (The WAMDI Group 1988). WAM is a spectral wave model that is discretized in frequency and direction and solves the numerical evolution of ocean waves as energy budgets based on the action density balance equation. The surface wind boundary conditions are forced using the ECMWF HRES atmospheric forecast. At the ocean boundary along 53°N latitude, wave lateral boundary conditions are directional

wave spectra from the ECMWF HRES wave forecast, also based on WAM. The ECMWF HRES atmospheric forecast has a regular longitude/latitude grid at 0.1 degrees. The ARC MFC wave–ice model has a spatial resolution of 3 km on the polar stereographic projection.

The sea-ice part of the ARC MFC wave–ice model is taken from the ARC MFC ocean analysis (the specific product name is ARCTIC\_ANALYSIS\_FORECAST\_PHYS\_002\_001\_A). The sea-ice model is the Community Ice Code and based on the viscous–plastic sea-ice rheology. The sea-ice model uses a one-thickness category sea-ice model based on the thermodynamics described by Drange & Simonsen (1996) and Sakov et al. (2012). There, the minimum thickness for the newly formed ice is given as 0.5 m. Implications of the minimum thickness value are evaluated with the buoy observations in a later section.

The Community Ice Code sea-ice model was coupled to the HYCOM. The atmospheric forcing is obtained from the ECMWF HRES atmospheric forecast. The data assimilation was performed weekly, using the ensemble Kalman filter (Sakov et al. 2012), for the following: altimeter sea level, in situ temperature and salinity profiles, the OSTIA sea surface temperature, OSI SAF SIC and drift observations, and the (winter) SIT from the CryoSat-2 and Soil Moisture and Ocean Salinity satellites. The HYCOM has a horizontal resolution of approximately 12 km, which is more than three times the resolution of the ARC MFC wave–ice model.

### **ECMWF HRES wave forecast**

Wave heights and periods from the ECMWF HRES wave forecast were used in this study as a tool to analyse the ARC MFC wave–ice model and the buoy observation comparison. The ECMWF HRES wave forecast was obtained for our research activity by the Arctic Data Archive System, Tokyo, Japan. We took a series of 0–24-hour forecasts to produce a time series during the observation period. The ECMWF HRES wave model accounts for sea ice using ice masks where grid cells with SIC > 0.30 are treated as land. The ECMWF HRES wave forecast model has a regular longitude/latitude grid at 0.125 degrees. The ECMWF HRES wave model is useful to evaluate the wave conditions in the open water near the ice edge based on the following premises. (1) When the wave evolution occurs entirely over the open water fetch, the ECMWF HRES wave and ARC MFC wave–ice models should agree. (2) Near the ice edge, where satellite-derived sea-ice data are uncertain, inaccurate sea-ice representation can cause erroneous wave predictions (Nose et al. 2020). (3) In such cases, the ECMWF HRES wave model that neglects sea ice may produce better predictions.

### **neXtSIM sea-ice model**

The neXtSIM sea-ice model (specific product name ARCTIC\_ANALYSISFORECAST\_PHY\_ICE\_002\_011; Rampal et al. [2016]; Ólason et al. [2022]) is a sea-ice product distributed by the CMEMS and based on the Brittle-Bingham-Maxwell rheology. Rampal et al. (2016) introduced this model describing that fracturing and faulting of sea ice should be expressed as an assembly of plates >O(1 km) and floes O(100 m), rather than an intact solid plate. The neXtSIM thermodynamical component is based on a three-category model that includes open water, newly formed ice and older ice, as described by Rampal et al. (2019). Rampal et al. (2016) show that their model calculates ice formation in the category of newly formed ice on the basis of the atmosphere and ocean forcing, whereas a prescribed growth rate is conventionally adopted in classical models (Rampal et al. 2016). The thickness range of this newly formed ice category is 0.05–0.275 m, which is considerably thinner than that of the ARC MFC ocean analysis.

Unlike the ARC MFC ocean model, neXtSIM is not coupled to an ocean circulation model but is coupled with a mixed-layer model that is relaxed to an ocean circulation model. The ocean part is represented by a single level “slab ocean” model of the mixed layer (Rampal et al. 2016) and uses the following daily averaged forcing from the TOPAZ4 ocean data assimilation model system: sea surface (0–3 m) ocean velocity, temperature and salinity, and the mixed layer depth (Williams et al. 2021). The atmospheric forcing is the ECMWF HRES atmospheric forecast, and the neXtSIM model assimilates OSI SAF SIC via the nudging scheme on a daily basis. Since the control variable is only the SIC, neXtSIM is strongly constrained to the observation, that is, the OSI SAF SIC. The model has a Lagrangian triangular mesh with an equivalent square grid resolution of ca. 7 km, for which the data are distributed on the 3 km polar stereographic projection grid.

### **The effects of sea ice on wave evolution as observed by the wave buoys and models**

#### **Sea ice as lateral boundary effects on wave evolution**

Significant wave height  $H_{m0}$  and period time series were extracted from the ARC MFC wave–ice model and the ECMWF HRES forecast at the Zeni-v2021 and SPOT-1386 positions during their deployment between 15 and 29 September 2021. The full time series for wave heights and periods are shown in Supplementary Figs. S2 and S3. In this subsection, we focus on the wave heights between

15 and 19 September immediately after the buoys were deployed in open water.

Following the deployment, the ECMWF HRES  $H_{m0}$  agrees well with both buoys for up to ca. 12 hours, whereas the ARC MFC  $H_{m0}$  is clearly underestimated (Fig. 5). Shortly after, however, the buoys'  $H_{m0}$  takes a steep decrease at about 14:00 on 15 September (Fig. 5), and the ECMWF HRES  $H_{m0}$  is overestimated, whilst the ARC MFC  $H_{m0}$  agrees qualitatively with the observation. This change coincides with the time when the Zeni-v2021  $H_{m0}$  began deviating slightly from that of SPOT-1386 (Fig. 3).

Immediately after the deployment at 06:00 on 15 September, the ARC MFC wave directions were primarily parallel to the ice edge (Fig. 6a). Tracing upwind from the buoys, the ice edge protrudes and shelters the buoys' effective fetch on which waves can grow. Considering the ARC MFC  $H_{m0}$  is underestimated, the ice edge sheltering of the buoys may be the cause of the underestimation, that is, the protruding ice edge may not be an accurate representation of the sea-ice field. For comparison, Supplementary Fig. S4c shows the buoys are not sheltered by any protruding ice edge features in the ECMWF HRES sea-ice representation.

The fetch orientation transitioned from along the ice edge to off-ice wave conditions (Fig. 6b) after the models' trend reversed. (Winds were also blowing from the ice cover [Supplementary Fig. S4b, d].) The ECMWF HRES  $H_{m0}$  is clearly overestimated (Fig. 6), and the ARC MFC  $H_{m0}$  agrees with the observations with a varying degree of predictability.

These observations demonstrate the lateral boundary effect that sea ice imposes on the wave fields. We conjecture that the inaccurate representation of the ARC MFC ice tongue imposed a lateral boundary condition that prohibited reproducing the true wave evolution when the fetch was orientated parallel to the ice edge. A similar scenario was also observed on 21 September 2021, in which the ice tongue representations between the ARC MFC and ECMWF HRES models were markedly different. This event is described in the Supplementary material to present further support to this conjecture.

### **Wave dissipation due to sea ice on 29 September**

South to south-easterly winds over the Laptev Sea generated on-ice waves on 29 September 2021. The model wave fields are shown in Fig. 7. By this time, both Zeni-v2021 and SPOT-1386 were in dense ice cover with SIC > 0.8 (see Fig. 3e). The ice edge geometry and wave orientation were not straightforward; the Zeni-v2021 location was downwind compared to the SPOT-1386, but the Zeni-v2021 distance to the ice edge relative to the wind direction was closer than that of SPOT-1386 (Fig. 7).

During this event, the ECMWF HRES wave model has no values at both buoys as they are covered by the ice mask. The ARC MFC wave–ice model simulates no waves at both buoys (Supplementary Fig. S2). However, the  $H_{m0}$  time series panel in Fig. 3c depicts that waves were observed at Zeni-v2021, reaching a peak  $H_{m0}$  value over 1.25 m. SPOT-1386 located ca. 30 km south-east of Zeni-v2021 did not observe any waves. To investigate how the wave energy propagated to the downwind Zeni-v2021, but not for SPOT-1386, we analysed the model representations of the sea-ice field of the ARC MFC ocean analysis and the neXtSIM sea-ice model product.

### **Sea-ice model representation differences and their effects on wave evolution**

#### **Comparison of ARC MFC and neXtSIM sea-ice field representations**

Sea-ice fields between ARC MFC and neXtSIM are compared at the buoys' location on 29 September 2021 in Fig. 8. It is apparent that the horizontal scale of ARC MFC sea-ice features (Fig. 8a, c) is effectively limited to the ARC MFC ocean analysis scale of ca. 12 km. This may be expected as interpolation to a high-resolution grid is unlikely to reveal features less than the original scale; the implication here is that there is an inconsistent scale between the wave–ice model geographical configuration and the model physics resolution. The scale of sea-ice features in the neXtSIM sea-ice model appears to be much finer; the reason for this may be speculated that the Lagrangian nature of the model can influence the thermodynamics as well as the mechanical properties.

Notwithstanding this, the striking differences between the two models pertaining to the buoys' wave observation are the ice edge location, the 0.80 SIC contour and the SIT differences. The neXtSIM SIC field shows that the distance from Zeni-v2021 to the sea-ice edge is much closer than shown in the ARC MFC field. Moreover, if we take the wave propagation as roughly 150 degrees, then 0.80 SIC ice-covered sea that the waves need to propagate to reach Zeni-v2021 is much shorter than that of the ARC MFC wave–ice model, whilst for SPOT-1386, this distance remains relatively similar. Regarding the sea-ice edge and 0.80 SIC contour differences between the ARC MFC ocean analysis and the neXtSIM sea-ice model, we revisit the data assimilation intervals and scheme differences: the ARC MFC ocean analysis assimilates data at weekly intervals and uses the ensemble Kalman filter with many control variables (see the earlier subsection about the ARC MFC wave–ice model), whereas the neXtSIM sea-ice model carries out daily

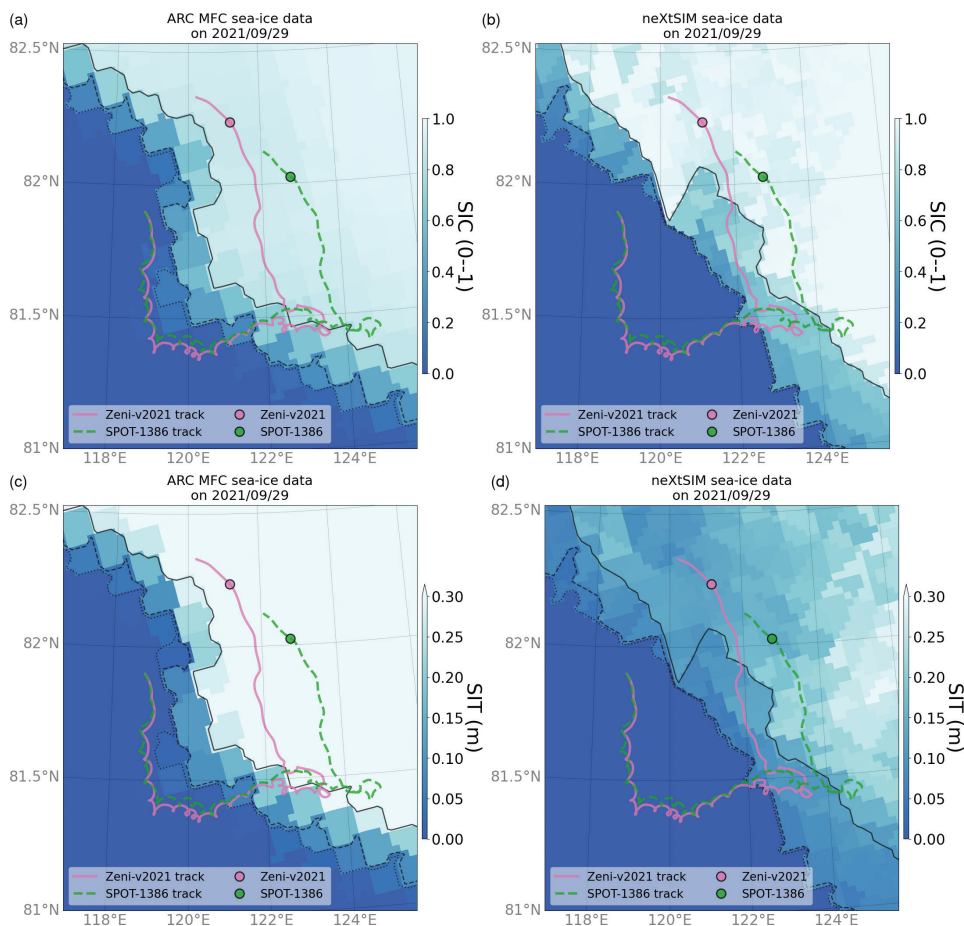


**Fig. 8** Comparison of ice conditions on 29 September 2021 between the (a) and (c) ARC MFC and (b) and (d) neXtSIM models. (a), (b) The SIC; (c), (d) the SIT. The SIC contour lines are 0.15 (dotted), 0.30 (dashed) and 0.80 (solid).

data assimilation via the nudging scheme with SIC being the only control variable (see the earlier subsection about the neXtSIM sea-ice model). The data here suggest that the differences in the data assimilation intervals and schemes produce diverging sea-ice field representations.

The representation of SIT in the ARC MFC model for thin ice appears to be poor: the ice field beyond the 0.80 SIC contour is practically  $SIT > 0.3$  m. By contrast, the neXtSIM SIT field clearly has a thickness distribution between 0 m and 0.3 m within the plot domain. The Supplementary material describes the observation-based ice chart that confirms the ice type near the ice edge, and the wave buoys were young ice. Although it is beyond the scope of this paper to examine whether coupling a wave model with the neXtSIM sea-ice forcing reproduces the co-located buoy data, there is sufficient evidence to suggest that the neXtSIM sea-ice representation appears to be in accord for reproducing the Zeni-v2021  $H_{m0}$ , that is, less dissipation because of low SICs and thinner thickness.

### Disparate scale between wave dissipation parameterization and the SIT forcing

The SIT disparity between the two models at the regional scale indicates that the ARC MFC SIT representation up to 0.5 m is poor (Supplementary Fig. S6). SIT is one of the most fundamental sea-ice variables, yet it remains difficult to measure as reliable methods are via ice core sampling, electromagnetic–induction instruments and select satellite observations (Tateyama et al. 2006; Tilling et al. 2018). In other words, regional/synoptic scale estimation of an SIT field is typically not readily available. For wave–ice models, an implication is that ice thickness can often serve as a wave dissipation tuning parameter. For ocean–ice coupled models, the essential feedback of sea ice to the ocean is thermodynamics, which is rather insensitive to thin ice. As such, one of the tuning parameters may be the minimum thickness parameter; indeed, the ARC MFC thermodynamic model is based on the work of Drange & Simonsen

(1996), which has the minimum thickness of newly formed ice as 0.5 m.

Another possibility for the poor thin ice representation is the data assimilation method. The AFC MFC ocean analysis is based on the ensemble Kalman filter scheme (Sakov et al. 2012) and does not assimilate SIT in the summer months. As shown in the previous section, the ice field beyond the 0.80 SIC contour in Fig. 8 is practically  $SIT > 0.3$  m; it is plausible that ARC MFC ocean analysis data assimilation may assume correlation between the observed SIC and unobserved SIT, which could be the cause of the poor thin ice representation.

From the wave–ice interaction viewpoint, however, pancake ice thickness is typically 5–10 cm, and new and young ice thickness is less than 30 cm (WMO 2021). The ARC MFC wave–ice interaction parameterization is based on the Sutherland et al. (2019) two-layer model, which parameterized the wave dissipation rate to scale with the SIT. Accordingly, the poor representation of MIZ thin ice cover in the sea-ice forcing is a critical issue. It appears, on the basis of Fig. 8 and Supplementary Fig. S6, that the ARC MFC ocean analysis does not resolve the thin thickness distribution that is appropriate for the wave dissipation model of Sutherland et al. (2019).

According to equation 16 by Sutherland et al. (2019),  $\varepsilon = 1$  determines the maximum dissipation in the moving viscous ice layer as  $\alpha = \frac{1}{2} h_i k^2$ . The maximum wave dissipation rates along the approximate wave propagation were plotted in Fig. 9 for the wave period of 7 s to quantify the effects of SIT differences between the ARC MFC and neXtSIM models. The SIT was extracted for 200 km along the approximate wave propagation ray from 121°E, 82.2°N on an initial bearing of 150 degrees. For relevance,

$T_p = 7$  s was roughly the upper limit of the co-located buoy observation when wave energy was detected (see Fig. 3). For SIT along the transect distance of 25–75 km, Fig. 9 shows that the ARC MFC wave dissipation rate can be three times than that of the neXtSIM counterpart. This figure confirms that the ARC MFC ocean analysis ice thickness does not adequately resolve the thin ice to apply the dissipation model of Sutherland et al. (2019); this prohibited a meaningful model–observation comparison to evaluate the Sutherland et al. (2019) model with our wave buoy observation: can their SIT-dependent dissipation rate reproduce waves in MIZ covered with thin ice?

For completeness, we conducted an academic experiment to show how the exponential dissipation rate  $\frac{dH_{m0}}{dx}$  differs because of poor thin SIT resolution. We used a Pierson Moskowitz spectrum with a 7.5 s  $T_p$  that has a 2.2 m  $H_{m0}$ . The dissipated  $H_{m0}$  was calculated from the spectrum  $S$  using Eqn. 2. Assuming a maximum dissipation rate over a 10 km distance with a thickness of 0.1 m and 0.5 m, we estimated  $H_{m0} = 0.1$  and 0.6 m, respectively. The difference of  $\frac{dH_{m0}}{dx}$  for the 0.5 m thickness results in 2.6 times the dissipation than the 0.1 m thickness case. However, it is difficult to know how this is reflected in the ARC MFC wave–ice model as the true SIC field, the sea-ice edge, and the incoming spectra shape are all unknown.

These considerations make it clear that the ARC MFC wave–ice model overestimated the wave dissipation in the thin ice fields with SIT less than 0.5 m during our buoy observation. The ARC MFC wave–ice model in MIZs near the ice edge needs SIT forcing that can resolve the thin ice types. It is worth mentioning that the neXtSIM sea-ice

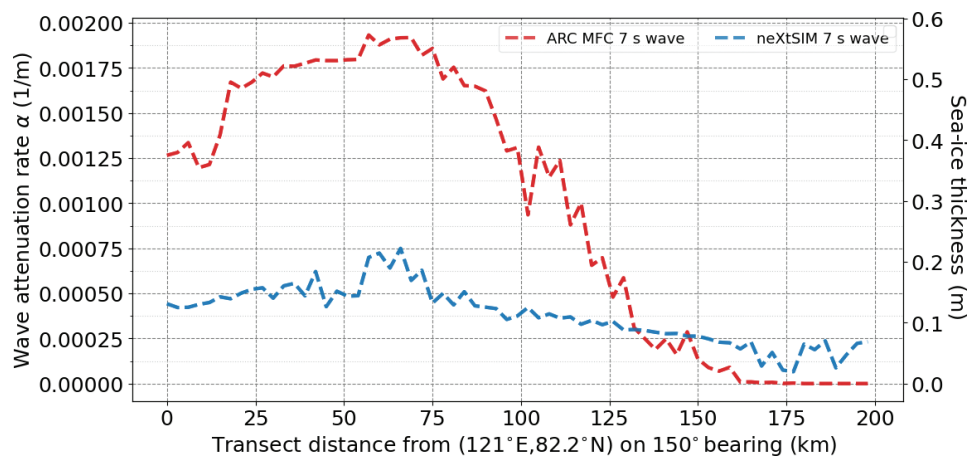


**Fig. 9** Comparison of Sutherland et al. (2019) wave dissipation rate  $\alpha = \frac{1}{2} \varepsilon h_i k^2$ , where  $\varepsilon = 1$  based on the ARC MFC and neXtSIM model SIT  $h_i$ .  $\alpha$  is plotted along a 200 km transect from 121°E, 82.2°N at an initial bearing of 150 degrees for waves with 7 s periods. The right axis is the SIT.

model has been experimentally coupled with the wave model of Boutin et al. (2021), though with a different viewpoint, their focus was the effect of waves on ice fragmentation utilizing the brittle rheology of neXtSIM.

## Conclusions

Two drifting wave buoys were deployed in the central Arctic Ocean, north of the Laptev Sea, where there have not been any wave observations available. The motivation for the buoy deployment was to validate the Zeni-v2021, a prototype of an experimental wave–ice buoy named OMB (Rabault et al. 2022), with SPOT-1386, a commercial wave buoy. The inter-buoy comparison showed that when the buoy distances between Zeni-v2021 and SPOT-1386 were close, defined here with the arbitrary threshold of 5 km, Zeni-v2021 was sufficiently accurate compared to the commercial SPOT-1386 buoy. As such, the buoy data were used to study the predictability of waves in the deployment region.

The first event we focused on occurred shortly after the deployment, when a sudden decrease in the buoys' significant wave heights  $H_{m0}$  from about 1.75 m to about 1.50 m was observed. The decrease coincided with the change in wind direction from along the ice edge to off-ice wind. The operational ARC MFC wave–ice model product did not reproduce the sudden decrease because the ice tongue constrained the wave growth over the available fetch. The analysis here shows the resolution of ice edge features is critically important for accurate predictions of waves in the nearby open water. The second case we analysed was when the wave buoys entered ice cover as new ice formed in the area. During this event, Zeni-v2021 located downwind of SPOT-1386 measured waves with a peak  $H_{m0}$  of 1.25 m, but SPOT-1386 did not detect any waves. The comparison of the buoy observation with the ARC MFC wave–ice model revealed that the ARC MFC wave–ice model largely underestimated the downwind Zeni-v2021  $H_{m0}$ . To elucidate the model error, we examined the model sea-ice conditions between the ARC MFC ocean analysis and the neXtSIM sea-ice model product. The analysis showed that the ARC MFC sea-ice forcing does not resolve thin thickness distribution for ice types like new and young ice, which are typically less than 30 cm thick. Since the ARC MFC wave–ice model's dissipation rate has an SIT dependence, the ARC MFC model overestimated wave dissipation in the thin thickness ice field. In contrast, neXtSIM seemed to resolve the thin thickness distributions in the MIZ. The model differences may be caused by new ice formation calculation methods and data assimilation schemes. Regardless of the cause, the ARC MFC wave–ice model

needs sea-ice forcing that reproduces thin ice cover for accurate predictions of ocean waves in MIZs when new ice is forming.

Reliable ocean wave forecasts are crucial for safe navigation in the polar seas. Our study presents an observational insight into the coupling of wave and ice models for better wave predictions in thin ice-covered MIZs. Observations and models help us ensure sustainable developments, such as safe navigation, in the changing Arctic Ocean.

## Acknowledgements

The authors sincerely thank 2021 NABOS chief scientist Dr Igor Polyakov for supporting their wave buoy deployment. The authors are grateful to Dr Guillaume Boutin and the anonymous reviewer for providing constructive criticisms during the peer review. Their invaluable comments led to a much improved manuscript. The authors are also grateful to CMEMS for providing a data distribution platform. The authors also sincerely thank the model developers of the ARC MFC wave–ice model and the neXtSIM sea-ice model products.

## Disclosure statement

The authors report no conflict of interest.

## Funding

Drs N. Kanna and K. Tateyama were supported by the ArCS II Japan-Russia-Canada International Exchange Program to participate in the 2021 NABOS expedition. This work was a part of the Arctic Challenge for Sustainability II (ArCS II) Project (program grant no. JPMXD1420318865). A part of this study was also conducted under JSPS KAKENHI grant nos. JP 19H00801, 19H05512, 21K14357 and 22H00241.

## References

- Arctic Data Archive System 2023. *AMSR2 Sea ice con. + sea surf. temp. + snow depth*. Accessed on the internet at <https://ads.nipr.ac.jp/vishop/#/extent> and plot 2012 and 2021 sea-ice extents on 5 May 2023.
- Bohlinger P., Carrasco A. & Saetra Ø. 2022. *Arctic Ocean wave analysis and forecast product ARCTIC\_ANALYSIS\_FORECAST\_WAV\_002\_014. Quality Information Document Issue 1.6*. Copernicus Marine Environment Monitoring Service.
- Boutin G., Williams T., Rampal P., Ólason E. & Lique C. 2021. Wave–sea-ice interactions in a brittle rheological framework. *The Cryosphere* 15, 431–457, doi: 10.5194/tc-15-431-2021.

- Drange H. & Simonsen K. 1996. *Formulation of air–sea fluxes in the Esop2 version of MICOM. Technical Report 125*. Bergen: Nansen Environmental and Remote Sensing Center.
- Hori M., Yabuki H., Sugimura T. & Terui T. 2012. *AMSR2 Level 3 product of daily polar brightness temperatures and product*. Version: 1.00. Arctic Data Archive System (ADS), Japan. Accessed on the internet at <https://ads.nipr.ac.jp/dataset/A20170123-003> on 1 Aug 2022.
- Linton C.M. 2010. Towards a three-dimensional model of wave–ice interaction in the marginal ice zone. *Journal of Fluid Mechanics* 662, 1–4, doi: 10.1017/S0022112010004258.
- NABOS. no date. *Nabos-II. Nansen and Amundsen Basins observational system. Report of the NABOS 2021 expedition. Activities in the Arctic Ocean. IARC Technical Report 11*. Fairbanks: International Arctic Research Center, University of Alaska Fairbanks.
- Nose T., Waseda T., Kodaira T. & Inoue J. 2020. Satellite-retrieved sea ice concentration uncertainty and its effect on modelling wave evolution in marginal ice zones. *The Cryosphere* 14, 2029–2052, doi: 10.5194/tc-14-2029-2020.
- Nose T., Webb A., Waseda T., Inoue J. & Sato K. 2018. Predictability of storm wave heights in the ice-free Beaufort Sea. *Ocean Dynamics* 68, 1383–1402, doi: 10.1007/s10236-018-1194-0.
- Ólason E., Boutin G., Korosov A., Rampal P., Williams T., Kimmritz M., Dansereau V. & Samaké A. 2022. A new brittle rheology and numerical framework for large-scale sea-ice models. *Journal of Advances in Modeling Earth Systems* 14, e2021MS002685, doi: 10.1029/2021MS002685.
- Rabault J., Nose T., Hope G., Müller M., Breivik Ø., Voermans J., Hole R.L., Bohlinger P., Waseda T., Kodaira T., Katuno T., Johnson M., Sutherland G., Johansson M., Christensen K.G., Garvo A., Jensen A., Gundersen G., Marchenko A. & Babanin A. 2022. OpenMetBuoy-V2021: an easy-to-build, affordable, customizable, open-source instrument for oceanographic measurements of drift and waves in sea ice and the open ocean. *Geosciences* 12, article no. 110, doi: 10.3390/geosciences12030110.
- Rampal P., Bouillon S., Ólason E. & Morlighem M. 2016. NeXtSIM: a new Lagrangian sea ice model. *The Cryosphere* 10, 1055–1073, doi: 10.5194/tc-10-1055-2016.
- Rampal P., Dansereau V., Ólason E., Bouillon S., Williams T., Korosov A. & Samaké A. 2019. On the multi-fractal scaling properties of sea ice deformation. *The Cryosphere* 13, 2457–2474, doi: 10.5194/tc-13-2457-2019.
- Sakov P., Counillon F., Bertino L., Lisæter K.A., Oke P.R. & Korabely A. 2012. TOPAZ4: an ocean–sea ice data assimilation system for the North Atlantic and Arctic. *Ocean Science* 8, 633–656, doi: 10.5194/os-8-633-2012.
- Squire V.A. 2018. A fresh look at how ocean waves and sea ice interact. *Philosophical Transactions of the Royal Society A* 376, article no. 20170342, doi: 10.1098/rsta.2017.0342.
- Squire V.A. 2020. Ocean wave interactions with sea ice: a reappraisal. *Annual Review of Fluid Mechanics* 52, 37–60, doi: 10.1146/annurev-fluid-010719-060301.
- Sutherland G., Rabault J., Christensen K.H. & Jensen A. 2019. A two layer model for wave dissipation in sea ice. *Applied Ocean Research* 88, 111–118, doi: 10.1016/j.apor.2019.03.023.
- Tateyama K., Shirasawa K., Uto S., Kawamura T., Toyota T. & Enomoto H. 2006. Standardization of electromagnetic–induction measurements of sea-ice thickness in polar and subpolar seas. *Annals of Glaciology* 44, 240–246, doi: 10.3189/172756406781811484.
- The WAMDI Group 1988. The WAM model—a third generation ocean wave prediction model. *Journal of Physical Oceanography* 18, 1775–1810, doi: 10.1175/1520-0485(1988)018<1775:TWMTGO>2.0.CO;2.
- Thomson J., Ackley S., Girard-Ardhuin F., Ardhuin F., Babanin A., Boutin G., Brozena J., Cheng S.K., Collins C., Doble M., Fairall C., Guest P., Gebhardt C., Gemmrich J., Graber H.C., Hold B., Lehner S., Lund B., Meylan M.H., Maksym T., Montiel F., Perrie W., Persson O., Rainville L., Rogers W.E., Shen H., Shen H., Squire V., Stammerjohn S., Stopa J. & Smith M.M. 2018. Overview of the Arctic Sea State and Boundary Layer Physics Program. *Journal of Geophysical Research—Oceans* 123, 8674–8687, doi: 10.1002/2018JC013766.
- Tilling R.L., Ridout A. & Shepherd A. 2018. Estimating Arctic Sea ice thickness and volume using CryoSat-2 radar altimeter data. *Advances in Space Research* 62, 1203–1225, doi: 10.1016/j.asr.2017.10.051.
- Wadhams P. 1975. Airborne laser profiling of swell in an open ice field. *Journal of Geophysical Research* 80, 4520–4528, doi: 10.1029/JC080i033p04520.
- Waseda T., Alberello A., Nose T., Toyota T., Kodaira T. & Fujiwara Y. 2022. Observation of anomalous spectral downshifting of waves in the Okhotsk Sea marginal ice zone. *Philosophical Transactions of the Royal Society A* 380, article no. 20210256, doi: 10.1098/rsta.2021.0256.
- Waseda T., Webb A., Sato K. & Inoue J. 2017. *Arctic wave observation by drifting type wave buoys in 2016*. ISOPE-I-17-569. San Francisco, CA: International Society of Offshore Polar Engineers.
- Waseda T., Webb A., Sato K., Inoue J., Kohout A., Penrose B. & Penrose S. 2018. Correlated increase of high ocean waves and winds in the ice-free waters of the Arctic Ocean. *Scientific Reports* 8, article no. 4489, doi: 10.1038/s41598-018-22500-9.
- Weber J.E. 1987. Wave attenuation and wave drift in the marginal ice zone. *Journal of Physical Oceanography* 17, 2351–2361, doi: 10.1175/1520-0485(1987)017<2351:waawdi>2.0.co;2.
- Williams T., Korosov A., Rampal P. & Ólason E. 2021. Presentation and evaluation of the Arctic Sea ice forecasting system neXtSIM-F. *The Cryosphere* 15, 3207–3227, doi: 10.5194/tc-15-3207-2021.
- WMO 2021. *Sea-ice information and services*. WMO 574. Geneva: World Meteorological Organization.